Long term experience with CsI photocathodes in gas photon detectors

2014 JINST 9 P01006

(http://iopscience.iop.org/1748-0221/9/01/P01006)

PUBLISHED BY IOP PUBLISHING FOR SISSA MEDIALAB

RECEIVED: *September 18, 2013*
ACCEPTED: *December 19, 2013*
PUBLISHED: *January 13, 2014*

Long term experience with CsI photocathodes in gas photon detectors

M. Alexeev,[a] **R. Birsa,**[a] **F. Bradamante,**[a,b] **A. Bressan,**[a,b] **S. Dalla Torre,**[a] **V. Duic,**[a,b] **M. Giorgi,**[a,b] **B. Gobbo,**[a] **S. Levorato,**[a,b] **A. Martin,**[a,b] **G. Sbrizzai,**[a,b] **P. Schiavon,**[a,b] **F. Sozzi**[a,1] **and F. Tessarotto**[a]

[a] *Istituto Nazionale di Fisica Nucleare (INFN) — Trieste section, Padriciano 99, 34149 Trieste, Italy*
[b] *University of Trieste, Department of Physics, via A. Valerio 2, 34127 Trieste, Italy*

E-mail: federica.sozzi@ts.infn.it

ABSTRACT: RICH-1 is a Cherenkov Imaging detector in operation at the COMPASS experiment at CERN SPS since 2001. MWPCs equipped with CsI photocathodes have been used as photon detectors, for the full detection area in the first years of operation, and for 75% of the area after a detector upgrade in 2006. The mean number of detected photons per particle has been extracted from the data collected during six years of COMPASS data taking. An indirect measurement of possible variations of the CsI quantum efficiency versus time is obtained from this analysis.

KEYWORDS: Wire chambers(MWPC, Thin-gap chambers, drift chambers, drift tubes, proportional chambers etc); Gaseous imaging and tracking detectors; Photon detectors for UV, visible and IR photons (gas) (gas-photocathodes, solid-photocathodes); Cherenkov and transition radiation

[1] Corresponding author.

doi:10.1088/1748-0221/9/01/P01006

2014 JINST 9 P01006

Contents

2014 JINST 9 P01006

1 Introduction

RICH-1 [1] is a large size gas-radiator Ring Imaging CHerenkov counter providing hadron identification to the COMPASS experiment [2] at CERN SPS. From 2001 to 2004, RICH-1 photon detection has been provided by MultiWire Proportional Chambers (MWPC) with CsI photocathodes [3, 4]. The photon detectors have been successively upgraded, and from 2006 onwards a faster detection system has been adopted. The central photon detector part is affected by the largest amount of uncorrelated background, and has been equipped with high time resolution MultiAnode PhotoMultiplier Tubes (MAPMT) [5]. In the peripheral region (75% of the active area) the MWPCs have been left unchanged, equipped with a new read-out system [6] based on the APV chip [7] to obtain better time resolution. CsI has a non negligible Quantum Efficiency (QE) in the far UV domain only, below 210 nm. It is the most robust solid-state photoconverting material among those typically used, thanks to a higher work function, while visible-light photoconverters are very fragile. CsI also exhibits a relative chemical robustness against oxygen and water, as compared to other photoconverters, especially visible-sensitive ones. These unique characteristics make it the obvious candidate as solide-state photocathode material in gas detectors: it has been chosen for the detectors developed within the R&D project RD26 [3, 4], resulting in the gas photon detectors used at COMPASS and in several other experiments [4, 8–11]. CsI is also the photoconverting material used by the novel gas photon detectors based on MicroPattern Gas Detector (MPGD) architectures. The first application is in the Hadron Blind Detector (HBD) [12] of the Phenix experiment at BNL. Its use is also planned in THick GEM (THGEM)-based photon detectors, introduced by A. Breskin and collaborators [13] and studied in detail for the upgrade of the hadron identification system [14] of the ALICE experiment at CERN LHC and for an upgrade of COMPASS RICH-1 [15]. In spite of the wide usage, the long-term CsI ageing issues in experimental conditions have not been deeply explored. The ageing due to the ion bombardment has been studied in accelerated tests, exposing

the detector to large integrated photon fluxes [16]: severe QE reduction is observed after collecting at the photocathode an integrated charge of a few mC/cm^2. Other possible ageing sources and, in particular, the long term stability have so far received limited attention. The availability of the COMPASS data collected over several years of data taking offers a unique opportunity to access the long term behavior of gas photon detectors equipped with CsI photocathodes. The CsI QE variation versus time has been studied monitoring the mean number of detected photons per incoming pion over six years of COMPASS data taking and the results are presented here. The article is organized as follows: COMPASS RICH-1 is shortly described in section 2; the characteristics of the data sample are given in section 3, the analysis of the data in section 4; section 5 contains the results of the analysis, and the systematic checks performed; conclusions are presented in section 6.

2 The RICH-1 detector

Figure 1 provides a scheme of principle and an artistic view of the detector. RICH-1 employs a gaseous radiator [17]: particles cross 3 m of C_4F_{10} mixed with a few percent of nitrogen. The gas pressure and its transparency in a wide wavelength range down to the UV domain, required by the photon detectors used, are crucial parameters for the correct detector operation. Image focusing is obtained thanks to a 21 m^2 wall formed by a mosaic arrangement of 116 spherical UV mirror elements [18]. The wall consists of two (upper and lower) spherical surfaces (nominal radius of 6600 mm) with different orientation (figure 1). A stainless steel pipe (diameter 100 mm) with its axis coinciding with the beam axis is present inside the radiator volume: it intercepts the Cherenkov photons produced by the beam particles. The 16 photon detector units shown in figure 1, eight forming the top detector set and eight the bottom set, experience quite diversified photon fluxes and detect the Cherenkov photons produced by particles with different momentum distributions. Correspondingly, two different photon detection techniques are used. The high momentum particles are detected in the central photon detection area, a region also highly populated by the uncorrelated background images. Therefore good resolution on the measured Cherenkov angle to rise towards momenta as high as possible the limit for hadron mass separation and fine time resolution to discriminate the uncorrelated background are required. The central region formed by the four most central detector units, two included in the top and two in the bottom detector set, is instrumented with a detection system based on MAPMT [5] coupled to individual telescopes of fused silica lenses to enlarge the acceptance and reduce the dead zone to about 2% only. In the peripheral region the photon flux is very low: the photodetection in this region, namely in the 12 external detector units, is performed with MWPCs equipped with solid state CsI photocathodes (cathodes in the following). Each cathode plane is a Printed Circuit Board (PCB) segmented into 8×8 mm^2 pads coated with a CsI film. The signals are collected from the photocathode pads. The active surface of each of the 12 photocathodes is 576×576 mm^2. A scheme of the detectors is shown in figure 2. The Cherenkov photons enter the chamber via a fused silica window and hit the photocathode PCB. The photoelectrons produced by the converted photons are multiplied in the MWPC. The amplification gas is pure methane and the pollutants are always kept below 5 ppm of oxygen and water vapour. The detectors are operated at low gain (below 5×10^4), as imposed by the presence of the CsI photocathode. In this peripheral region the photon and ionizing particle flux is low: both fluxes are less than 10 Hz/cm^2 during the SPS spill. The photon detectors are

2014 JINST 9 P01006

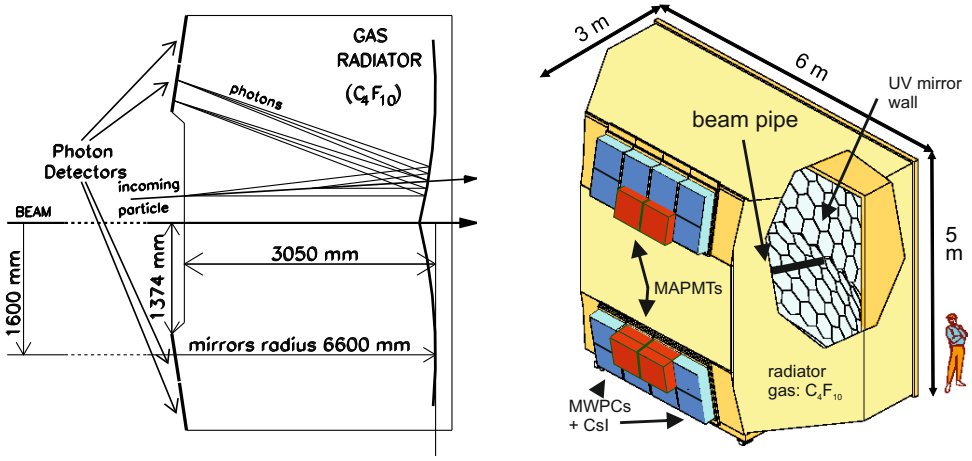

Figure 1. A scheme of principle and an artistic view of the RICH-1 detector.

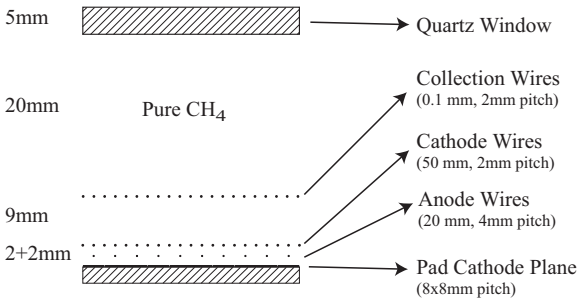

Figure 2. Schematic cross-section of the COMPASS RICH-1 gaseous photon detectors (not to scale).

out of the experiment acceptance, and thus no continuous monitoring of the particle rates in this region is possible. Nevertheless, dedicated measurements with scintillation counters performed with different beam conditions allow to put an upper limit to these fluxes. The resulting integrated ion backflow flux over the six years considered in the present study is smaller than 10 μC/cm^2, namely more than two orders of magnitude lower than the integrated photocathode bombardment flux causing the QE reduction reported in literature. In the following, to extract the information about the detected Cherenkov photons emitted by an ionizing particle crossing the RICH-1 radiator, the information provided by a pattern recognition algorithm is used [19]. A cluster is defined grouping the maximum pulse height pad with the adjacent pads with a pulse height below a certain percentage of the maximum value. The impact point of the cluster is defined as the mean of the pad positions, weighted with the pulse height. To define the pseudo ring images, the distribution of the cluster Cherenkov angles relative to a track is scanned using a window, whose width is typically twice the single photon resolution sigma. The window corresponding to the largest content of clusters defines the ring. The number of detected photons associated to a ring includes all the clusters in an annulus 4-sigma wide.

2014 JINST 9 P01006

3 Data sample

Samples from the 2006 to 2011 COMPASS data have been used for this analysis, in order to compare samples collected using the same read out electronics. Each sample includes the data collected over several days, up to 15: the samples ensure negligible statistical errors. Each year is characterized by different data taking conditions, including different triggers, targets and beams. In particular, in two years (2008 and 2009) data dedicated to hadron spectroscopy have been collected with hadron beams, while in the other 4 years polarised semi-inclusive deep inelastic scattering measurements have been performed using muon beams. To select samples as homogeneous as possible, in spite of different experimental conditions, the same cuts have been applied to the reconstructed particle trajectories. The selected tracks have an associated Cherenkov ring, and have been identified as pions using particle identification criteria based on a likelihood analysis [19].

The non-homogeneity of the data introduces differences in the amount and distribution of the background photons in the detectors, due to the different particles multiplicity and phase space. This difference is taken into account in the analysis, where the signal and background contribution to the ring are separated (section 4).

Some systematic effects can be also introduced by changes of the RICH parameters, as MWPC HV and electronics settings, and the radiator composition. The MWPC HV values are the same for the first 4 years analysed, while they have been decreased by 20V in the last 2 years. A correction for this reduction has been evaluated from the plot of gain variation with HV, measured in laboratory, and has been applied in the last part of the analysis, described in section 5. The electronic noise level in the cathodes is taken into account due to the procedure used to evaluate the background in the photon ring. The difference due to the electronics settings, calibrations and in the gas transparency, namely the absorption of photons, are small and quantitatively discussed in section 5.

The tracks with an associated ring contained in the MWPC detectors are characterized by low momenta. Figure 3 shows the track momentum distribution for each of the 12 MWPC cathodes. The position of the histograms correspond to the position of the MWPC cathodes in the detector: the 2 top rows correspond to the upper photon detector, the 2 bottom rows to the lower one. The 4 cathodes in the corners (n. 1, 4, 13, 16) are populated by the smallest momentum particles, due to their geometrical position matching the largest polar angles. The different population between the 4 off-corner cathodes in the top and bottom part (n. 2, 3, 14, 15) with respect to the 4 in the left and right part (n. 5, 8, 9, 12) is due to the deflection in the horizontal plane introduced by the spectrometer magnet positioned upstream of RICH-1 and the mirror orientation. Due to the low momentum values, most of the tracks do not reach the maximum values of the Cherenkov angle (around 53 mrad), as can be seen from the distribution shown in figure 4.

4 Data analysis

Only rings fully contained in a single cathode are considered, in order to have twelve independent data sets. For each ring the number of photons and their mean Cherenkov angle, namely the ring angle θ_{Ch}, are considered. For the following analysis, the data are grouped in 1 mrad wide θ_{Ch} bins, and for each of them the mean value of the corresponding distribution of the number of photons is evaluated.

2014 JINST 9 P01006

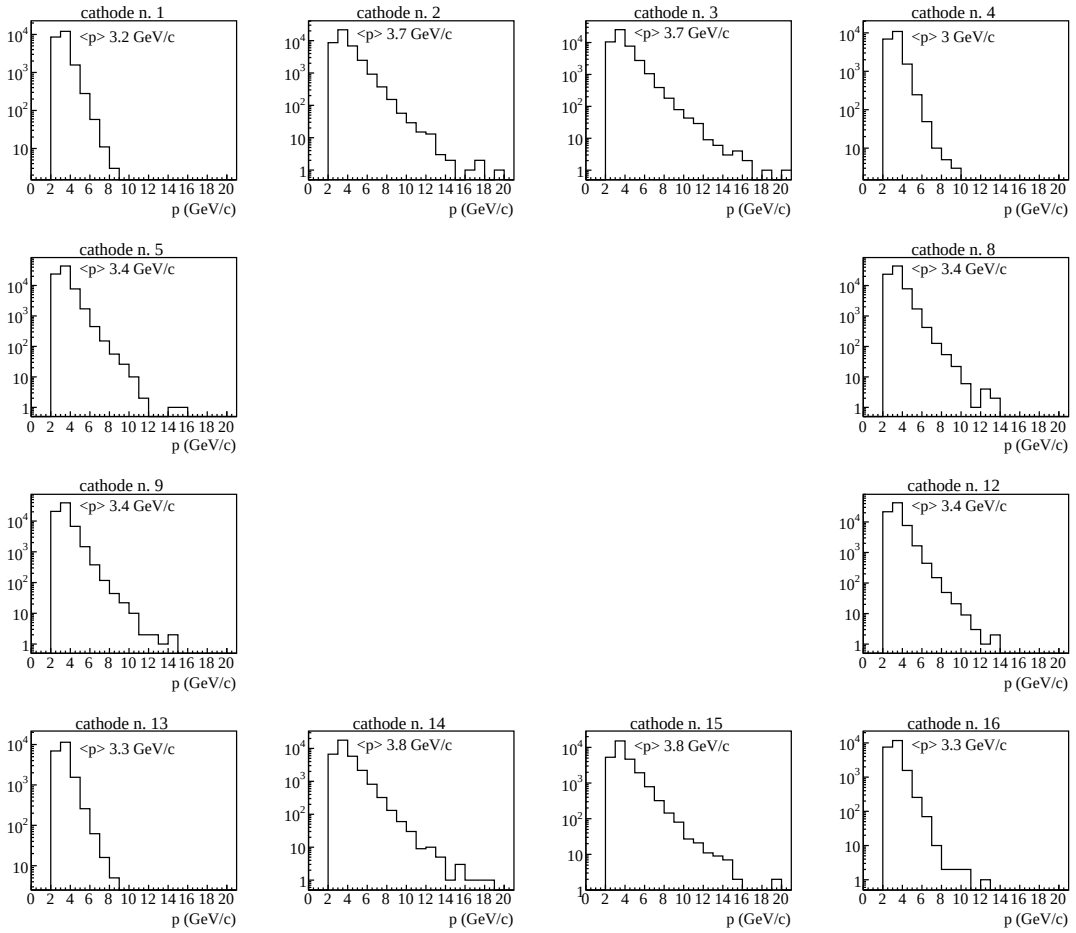

Figure 3. The momentum distribution of the particles with a ring fully contained in each of the twelve RICH MWPC cathodes. Sample from 2006 data.

The number of emitted Cherenkov photons follow a Poissonian statistics. In the following we assume that also the number of detected Cherenkov photons follow the same distribution, despite the ring reconstruction algorithm, the detection issues and the presence of the background photons could in principle modify the distribution. Since the particle trajectories are reconstructed, the minimum requirement to have a reconstructed ring is to have at least one associated photon. This fact implies that the poissonian distribution of the number of photons is not complete because zero-photon rings are not taken into account: the mean value is biased towards larger values. This bias is evaluated in appendix A and is different for Poissonian distribution with different mean values, increasing for low mean values. This implies that the bias is not a simple offset in the distribution of the number of photons versus $\theta_{\rm Ch}$, but also modifies the distribution shape. Figure 5 shows an example of distribution of the mean number of photons per ring as a function of the Cherenkov angle, with and without applying the bias correction. After correction, the number of photons goes to zero at small $\theta_{\rm Ch}$ values, as expected. In order to check the validity of the approach, the distributions obtained requiring a minimum number of photons equal to 1, 2 and 3, have been corrected for the corresponding bias (see appendix A) and compared. The histograms are very similar. A small residual systematic effect is visible in the small angle region, while it

2014 JINST 9 P01006

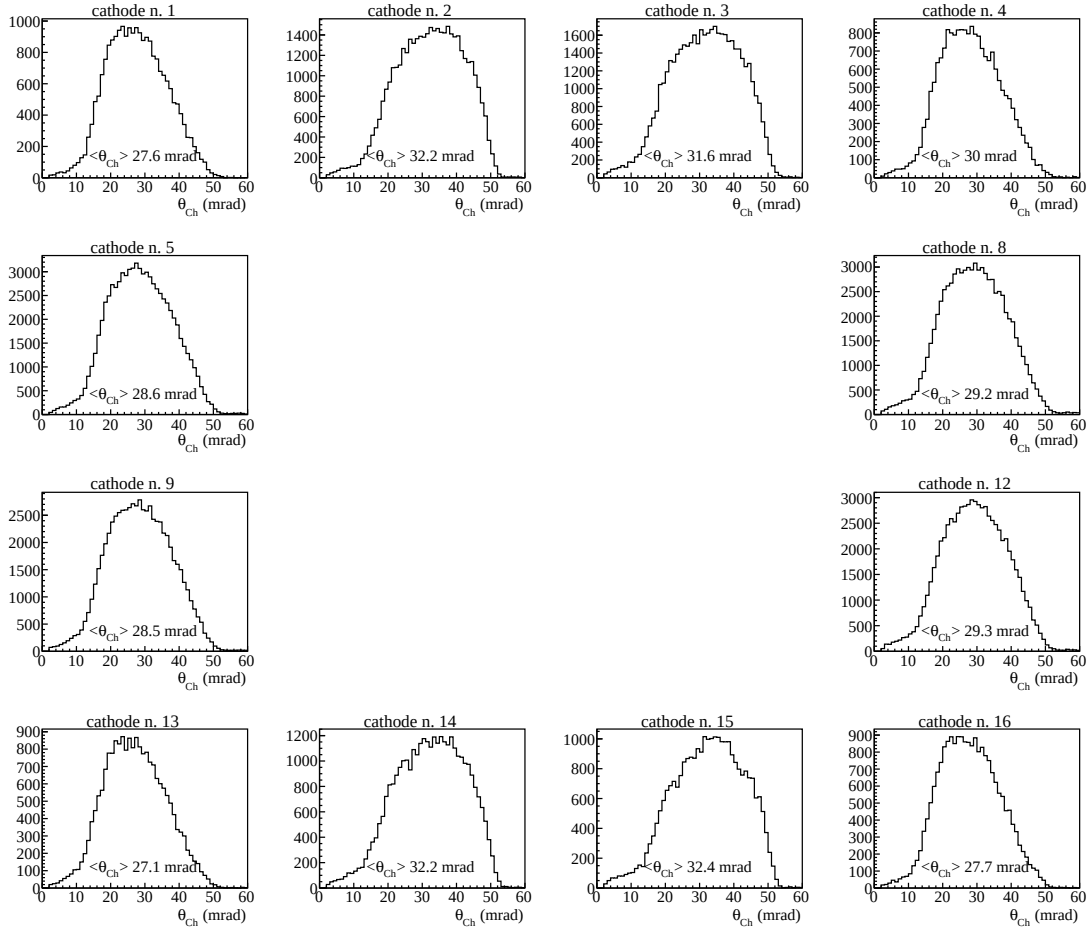

Figure 4. The Cherenkov angle distribution of the particles with a ring fully contained in each of the twelve RICH cathodes. Same data sample of figure 3.

is negligible above 25 mrad. For the following analysis, rings with at least one photon are used and the distributions are corrected for the bias. Rings with the minimum requirement of 2 and 3 photons are used for systematic checks (section 5).

The distributions of the average number of photons versus $\theta_{\rm Ch}$ are fitted with the following function:

$$N(\theta_{\rm Ch}) = p_0 \cdot sin^2\theta_{\rm Ch} + p_1 \cdot \theta_{\rm Ch} \tag{4.1}$$

The first term describes the number of signal photons following a Frank and Tamm shape. The second term describes the background contribution with a linear $\theta_{\rm Ch}$ dependence as suggested by geometrical considerations: the data show that the background photons are distributed uniformly in the cathodes. It is required that the two free parameters p_0 and p_1 have non negative values, considering their physical meaning.

In order to compare the results coming from different years, the number of the signal and the background photons is evaluated at a fixed value of $\theta_{\rm Ch}$: the Cherenkov angle at saturation in the 2006 data ($\theta_{\rm Ch}^{\rm max} = 55.2 mrad$).[1] In fact the number of Cherenkov photons is proportional to

[1]The saturation values vary in the range [53.3-55.4] mrad in the different years, due to the different fraction of

2014 JINST 9 P01006

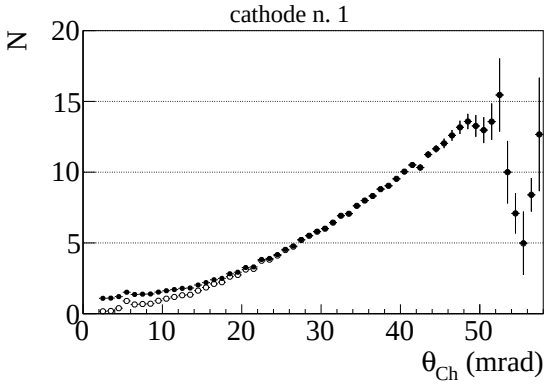

Figure 5. Distribution of the mean number of photons per ring as a function of the Cherenkov angle, with (open circles) and without (closed circles) applying the Poissonian correction. The Cherenkov angle distribution does not reach the saturation value due to the momentum distribution, as illustrated in figures 3 and 4 . The decreasing distribution slope above 50 mrad is due to the finite resolution affecting the measured Cherenkov angle.

$\sin^2\theta_{\rm Ch}$: by evaluating it at a fixed value of $\theta_{\rm Ch}$, the variation due to small variations of the index is removed.

The lower limit of the fitted region is set to 25 mrad, in order to have a negligible residual effect from the Poissonian correction. The upper limit is set subtracting a fixed value from $\theta_{\rm Ch}^{\rm max}$: this value is 15 mrad for the corner cathodes, and 10 mrad for the others.

As an example, the distributions of the number of photons in the twelve cathodes as a function of the Cherenkov angles are shown in figure 6, for year 2006. The resulting mean number of signal and background photons, N_S and N_B, as well as the reduced χ^2 of the best fit procedure and the corresponding probabilities are indicated in the plots.

5 Results

The mean number of signal and background photons evaluated at 55.2 mrad (section 4) from the best fit procedure for the different RICH cathodes are shown for the six years in figure 7. In general the fits are good, for all the cathodes and the years, apart for the cathode n. 15 located in the bottom part of the detector. For this cathode, the number of background photons reaches the constraint value of zero in the last three years and the corresponding χ^2 is high. This cathode is known to be electrically unstable, and the number of detected photons is too low to be properly described by the fit function. This cathode is thus removed from the following analysis.

In order to investigate the presence of systematic effects, the distribution of the χ^2 from the best fit procedure has been checked. Figure 8 shows the distribution for the 7 off-corner cathodes, compared with the expected distribution of a χ^2 with a Number of Degrees of Freedom (NDF) equal to 18. The shape is similar, while the values are slightly shifted. From the shift of the mean value, we evaluate a systematic error of 0.7 of the statistical one, σ_{stat}. The same test for the corner cathodes, in which the fits have NDF equal to 13, gives an estimate of a systematic error of 0.4 of

nitrogen contamination in the gas, which is the main source of different values of the refractive index.

2014 JINST 9 P01006

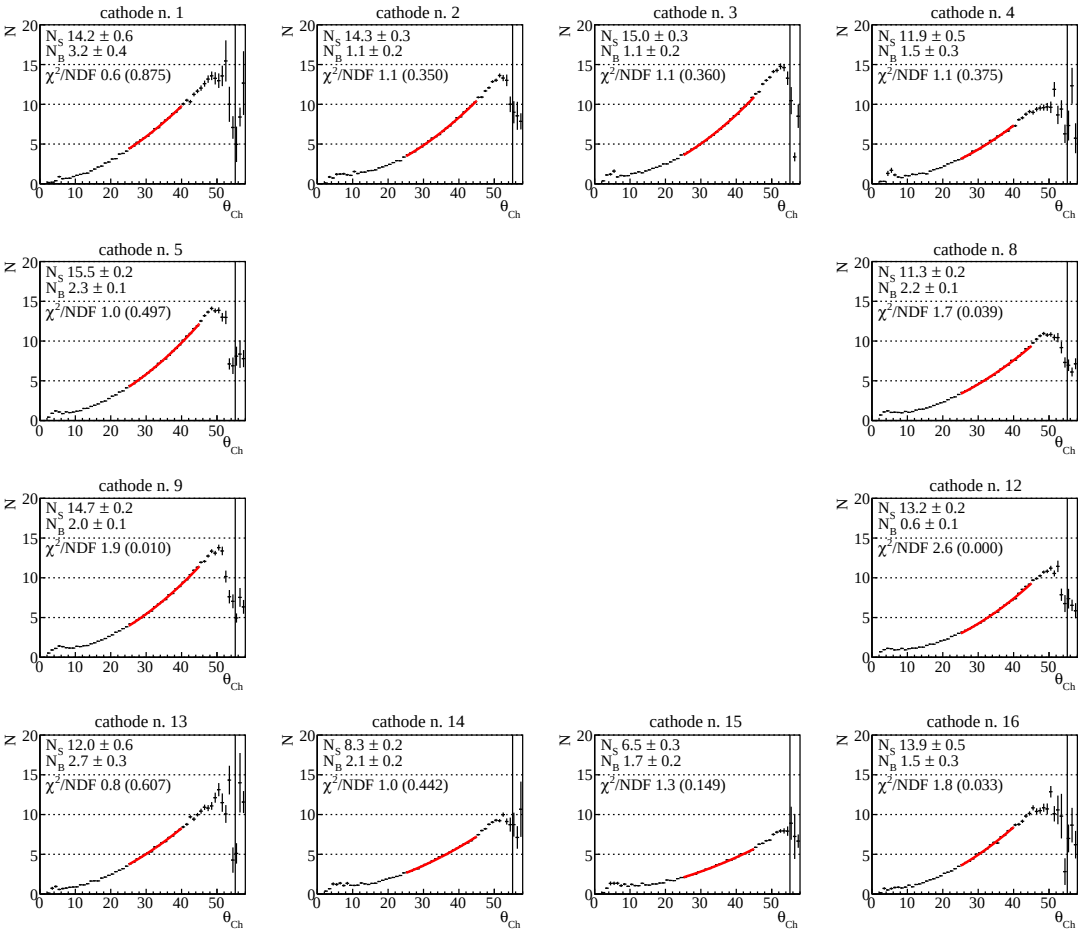

Figure 6. Distributions of the number of photons as a function of the Cherenkov angle, for each cathode. The result of the best fit procedure is shown as the red bold line superimposed to the graph. The vertical line indicates the saturation angle θ_{Ch}^{max}, at which the number of signal and background photons are evaluated.

the statistical error, an higher absolute value since the statistical error in these cathodes is larger of a factor 3.

The mean value of the 11 graphs is shown in figure 9. The error bars represent the statistical plus the systematic contribution, set to the largest found in the χ^2 fit test. Another source of systematic errors investigated is the range used in the fit. Figure 10 shows the mean number of signal and background photons obtained from three fits in which the lower limit has been varied in the range 15-25 mrad. A very good agreement between the results is visible. The possible influence of the Poissonian correction to the results has been investigated performing the same analysis on samples of rings with the requirement of a number of photons larger than 1 and 2. The results are compared with the standard ones in figure 11. It can be seen how the 3 sets of results differ mainly when the number of photons is low. This can be understood since in these cases the requirement of at least 2 or 3 photons changes substantially the ring sample population. This results in a small offset between the three mean values of signal and background photons shown in figure 11. Nevertheless, the shape of the three curves is the same, so that the quantity of interest for this study, namely the variation versus time, is not affected. The sources of systematic

2014 JINST 9 P01006

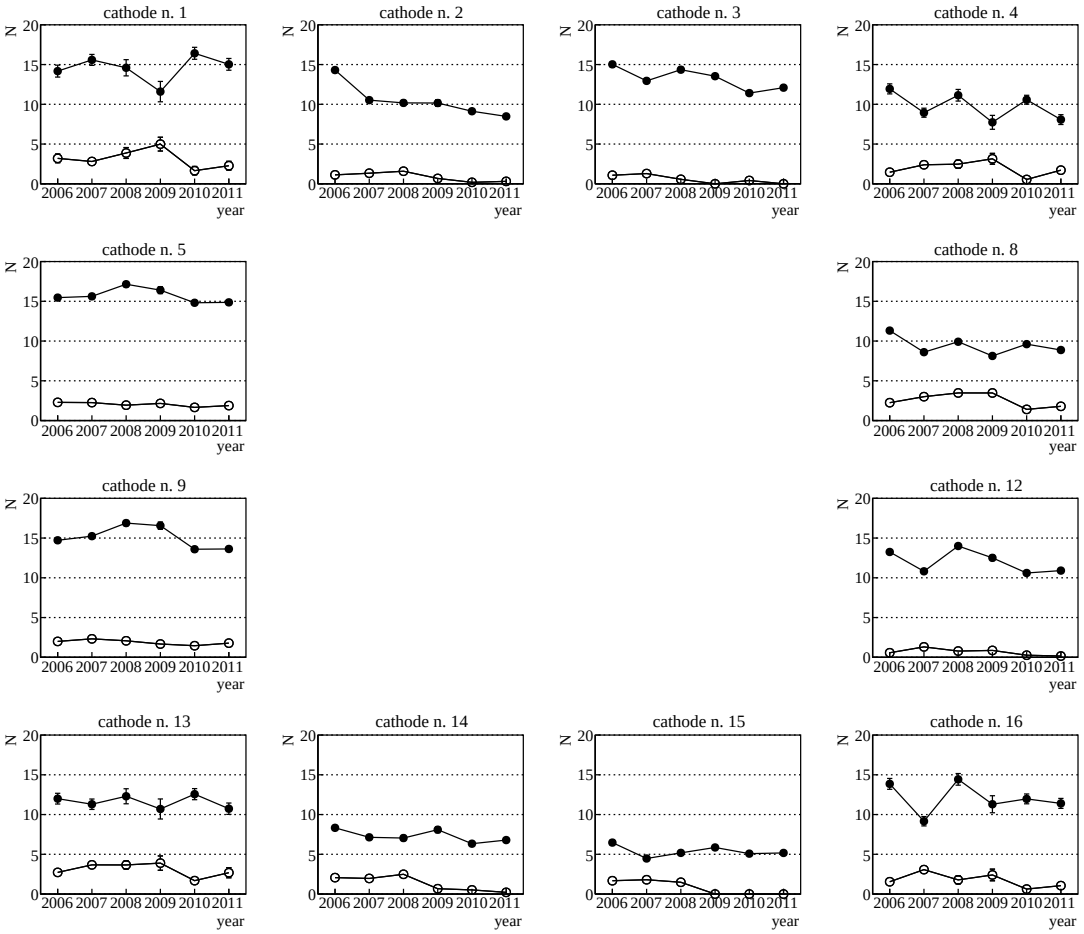

Figure 7. Distributions of the number of signal (closed points) and background (open points) photons as a function of year, for each cathode.

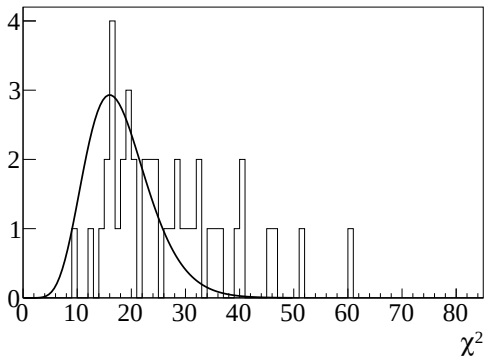

Figure 8. χ^2 distribution of the best fit procedure applied to the data of the 7 off-corner cathodes, compared with the theoretical curve for 18 degrees of freedom.

effects that can affect the comparison of the data samples have been carefully analysed. The use of different beams and data taking conditions can result in different signal over background ratio. The function used to fit the data allows to determine the two contributions separately in order to

2014 JINST 9 P01006

Figure 9. Mean value over the 11 cathodes of the number of signal (closed points, top curve) and background (open points, bottom curve) photons versus the year.

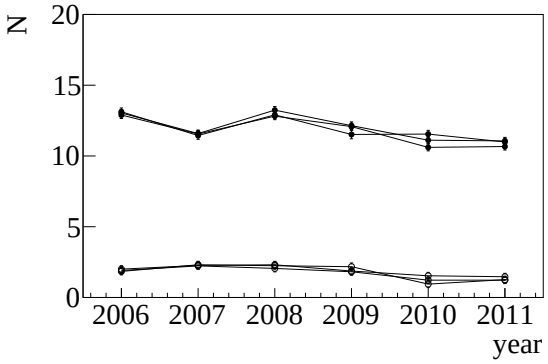

Figure 10. Distributions of the mean value over the 11 cathodes of the number of signal (closed points, top curves) and background photons (open points, bottom curves) as a function of year. The different graphs correspond to different minimum range values for the fit, ranging from 15 to 25 mrad.

extract the signal not affected by the background contribution. Each data sample is collected over several days during which the temperature at the detector and the atmospheric pressure vary. The average temperature and pressure values are evaluated for each data sample. The r.m.s. values of the resulting variation of the number of detected photons are 1% and 0.6% respectively. Similarly the effect of the different electronic threshold settings for the various years introduces a dispersion in the number of detected photons with r.m.s. equal to 0.7%. The variation of the refractive index is not completely negligible, but it does not affect the results thanks to the extrapolation of the fitted functions to the same value of the Cherenkov angle for each data sample. No variation of the gas transparency has been observed within the resolution of the measurements [1].

The trend shown in the plot of figure 9 gives no evidence for a substantial decrease of CsI QE in time. Moreover the last two points have been collected with a decrease of 20V in the HV. The corresponding correction factor, of about 2.3%, has been applied for the final step of the analysis, and the corrected points are shown in figure 12. A fit with a first order polynomial gives a slope of about -0.28 photons/year, corresponding to a decrease rate of 2.3% per year. The confidence level of the fit is very small, likely due to missing independent contributions to the systematic error, as mentioned in section 3. In figure 12 the points are thus presented with enlarged error bars, set in

2014 JINST 9 P01006

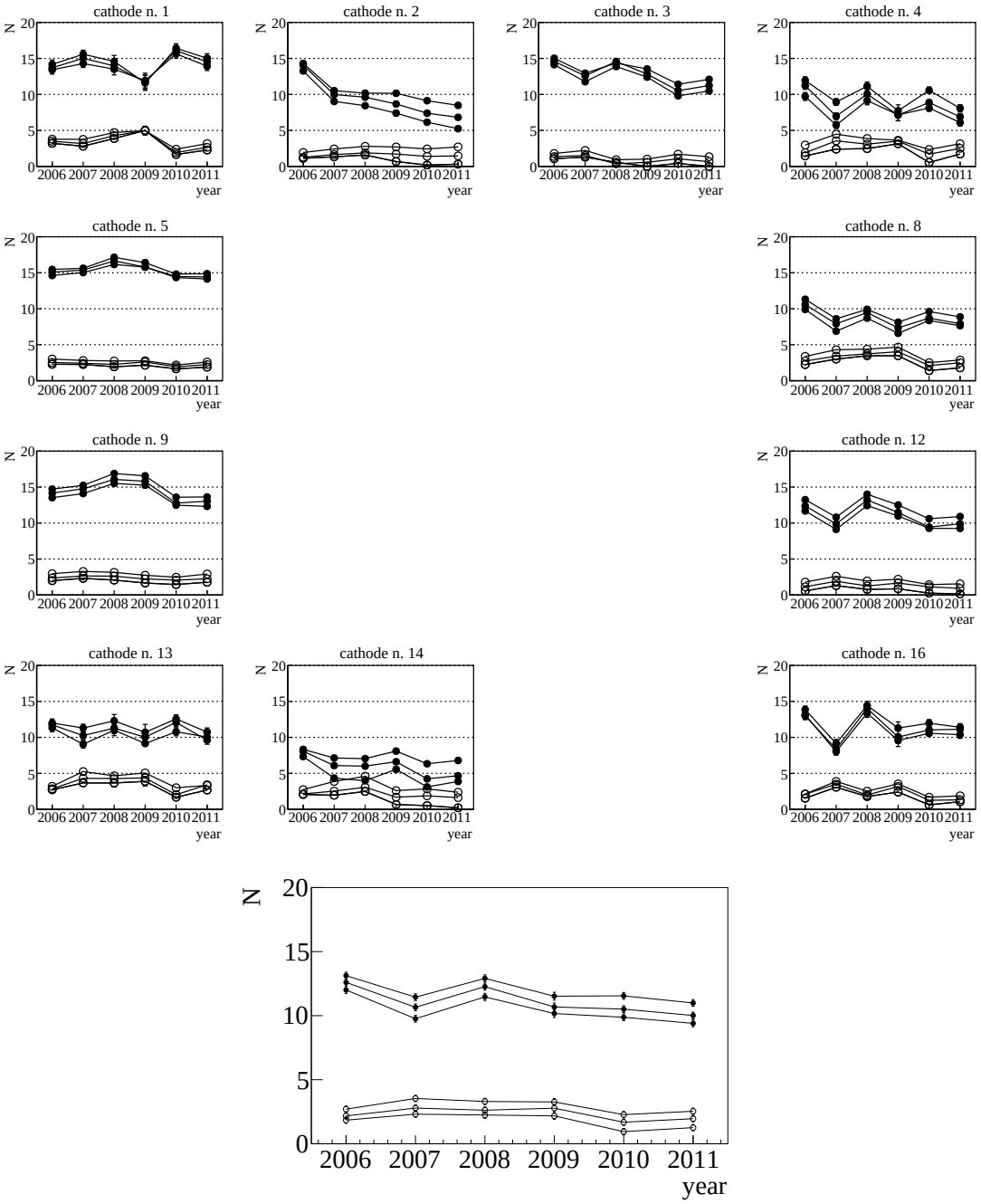

Figure 11. Distributions of the number of signal (closed points) and background (open points) photons as a function of year. The different graphs correspond to requirement of 1, 2 or 3 minimum photons for ring. In the top part the distribution for each cathode, in the bottom the mean value over the 11 cathodes.

order to reach 0.5 probability in the first order polynomial fit. The 6 points with the enlarged errors are also fitted with a constant value, giving a CL of 33.4%, thus this hypothesis is not rejected on statistical basis. The slope of -0.28 photons/year can be taken as an upper limit of the decrease of the CsI QE. Nevertheless, single cathodes exhibit a QE decrease: from the average value of n. 2, 3 and 14 the slope is -0.54 photons/year, corresponding to 5.2% per year.

2014 JINST 9 P01006

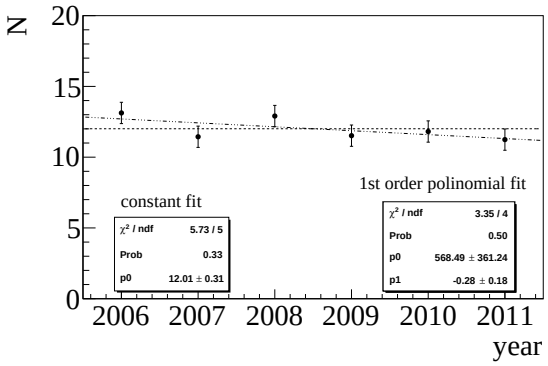

Figure 12. Mean number of signal photons as a function of the year. The last two points have been corrected for the HV decrease and the error bars are larger with respect to those in figure 9, as explained in the text. Results from the best fit procedure with a constant (dashed line) and a first order polynomial function (dotted-dashed line) are shown.

6 Conclusions

We report about the variation of the QE of the CsI photocathodes equipping the COMPASS RICH-1 gas photon detectors over a period of six years.The detectors are operated with pure methane and the pollutants are always kept below 5 ppm of oxygen and water vapour. The gain is moderate, lower than 5×10^4 and the integrated ion charge collected at the photocathode is modest, less than 10 μC/cm^2. The data do not indicate any severe ageing effect: globally they are compatible with the hypothesis of no QE variation and suggest a maximum QE decrease rate of 2.3% per year. Nevertheless, a subset of photocathodes indicate a QE decrease at moderate rate: 5.2% per year.

The most natural hypothesis to explain a possible decrease with time of the CsI QE in gas photon detectors is a chemical or morphological evolution of the CsI film. This evolution can be related to the oxygen and water vapour contamination to which the photocathodes are exposed over years. In this hypothesis, the larger effect suggested by the data of a subset of cathodes can be caused by a local larger contamination level. No data of the contamination level in the individual detectors is available because the contamination is monitored only on a global base.

From this analysis, we conclude that CsI photocathodes used in gas photon detectors are robust and, if correctly operated, they can preserve their QE over period of years with at most a modest decrease.

A Evaluation of the Poissonian correction

The number of photons per ring is assumed to follow a poissonian distribution $P(k,\mu)$ with mean value μ. Considering rings with a number of photons larger or equal than a minimum value *nc*, the corresponding distribution is modified into $P^{'}(k,\mu^{'})$:

$$P^{'}(k,\mu^{'}) = \frac{P(k,\mu)}{\sum_{k=nc}^{\infty} P(k,\mu)} \tag{A.1}$$

2014 JINST 9 P01006

The modified mean value $\mu^{'}$ is evaluated as:

$$\mu^{'} = E[k] = \sum_{k=nc}^{\infty} kP^{'}(k,\mu) \tag{A.2}$$

$$= \frac{\sum_{k=nc}^{\infty} kP(k,\mu)}{\sum_{k=nc}^{\infty} P(k,\mu)} \tag{A.3}$$

$$= \frac{\sum_{k=0}^{\infty} kP(k,\mu) - \sum_{k=0}^{nc-1} kP(k,\mu)}{\sum_{k=0}^{\infty} P(k,\mu) - \sum_{k=0}^{nc-1} P(k,\mu)} \tag{A.4}$$

$$= \frac{\mu - \sum_{k=0}^{nc-1} kP(k,\mu)}{1 - \sum_{k=0}^{nc-1} P(k,\mu)} \tag{A.5}$$

The formulas corresponding to a minimum number of photons in the ring of 1, 2 and 3 are as follow:

$$\mu^{'}(nc=1) = \frac{\mu}{1-e^{-\mu}} \tag{A.6}$$

$$\mu^{'}(nc=2) = \frac{\mu(1-e^{-\mu})}{1-e^{-\mu}(1+\mu)} \tag{A.7}$$

$$\mu^{'}(nc=3) = \frac{\mu(1-e^{-\mu}) - \mu^2 e^{-\mu}}{1-e^{-\mu}(1+\mu+\frac{\mu^2}{2})} \tag{A.8}$$

The correction is applied evaluating the real mean value μ from the measured $\mu^{'}$, solving numerically the equations above.

Acknowledgments

The authors are grateful to the colleagues of the COMPASS Collaboration for constant encouragement and support and the permission to use the COMPASS data.

References

[1] E. Albrecht et al., *Status and characterisation of COMPASS RICH-1*, *Nucl. Instrum. Meth.* **A 553** (2005) 215.

[2] COMPASS collaboration, *COMPASS: a proposal for a Common Muon and Proton Apparatus for Structure and Spectroscopy*, CERN-SPSLC-96-14 (1996); *COMPASS: Common Muon and proton apparatus for Structure and Spectroscopy*, CERN-SPSLC-96-30 (1996).

[3] RD26 collaboration, *Status report from the CsI-Rich collaboration: R&D for the development of a large area advanced fast rich detector for particle identification at the LHC operated with heavy ions: RD-26*, CERN-DRDC-93-36 (1993); *Status report of the CSI-RICH collaboration 1994: development of a large area advanced fast RICHC detector for particle identification at the LHC operated with heavy ions*, CERN-DRDC-94-49 (1994); *RD26 status report*, CERN-DRDC-96-20 (1996);
F. Piuz, *Ring imaging cherenkov systems based on gaseous photo-detectors: trends and limits around particle accelerators*, *Nucl. Instrum. Meth.* **A 502** (2003) 76.

[4] ALICE collaboration, *Technical design report of the high momentum particle identification detector*, CERN-LHCC-98-19 (1998).

2014 JINST 9 P01006

[5] P. Abbon et al., *Design and construction of the fast photon detection system for COMPASS RICH-1*, *Nucl. Instrum. Meth.* **A 616** (2010) 21.

[6] P. Abbon et al., *Design and status of COMPASS FAST-RICH*, *Nucl. Instrum. Meth.* **A 567** (2006) 114.

[7] M.J. French et al., *Design and results from the APV25, a deep sub-micron CMOS front-end chip for the CMS tracker*, *Nucl. Instrum. Meth.* **A 466** (2001) 359.

[8] C.W. Fabjan et al., *The TIC: a multiparticle threshold imaging Cherenkov detector*, *Nucl. Instrum. Meth.* **A 367** (1995) 240;
M. Spegel, *The impact of the TIC on the physics performance of NA44*, *Nucl. Instrum. Meth.* **A 433** (1999) 366.

[9] J. Friese et al., *Enhanced quantum efficiency for CsI grown on a graphite based substrate coating*, *Nucl. Instrum. Meth.* **A 438** (1999) 86;
H. Rabus et al., *Quantum efficiency of cesium iodide photocathodes in the 120-220 nm spectral range traceable to a primary detector standard*, *Nucl. Instrum. Meth.* **A 438** (1999) 94;
R. Gernhäuser et al., *Cesium iodide photon converter performance in a gaseous RICH detector*, *Nucl. Instrum. Meth.* **A 438** (1999) 104.

[10] A. Braem et al., *Identification of high p_T particles with the STAR-RICH detector*, *Nucl. Instrum. Meth.* **A 499** (2003) 720.

[11] F. Garibaldi et al., *A proximity focusing RICH detector for kaon physics at Jefferson Lab Hall A*, *Nucl. Instrum. Meth.* **A 502** (2003) 117;
M. Iodice et al., *Performance and results of the RICH detector for kaon physics in Hall A at Jefferson Lab*, *Nucl. Instrum. Meth.***A 553** (2005) 231.

[12] W. Anderson et al., *Design, construction, operation and performance of a hadron blind detector for the PHENIX experiment*, *Nucl. Instrum. Meth.* **A 646** (2011) 35 [arXiv:1103.4277].

[13] A. Breskin et al., *A Concise review on THGEM detectors*, *Nucl. Instrum. Meth.* **A 598** (2009) 107 [arXiv:0807.2026].

[14] A. Di Mauro et al., *The VHMPID RICH upgrade project for ALICE at LHC*, *Nucl. Instrum. Meth.* **A 630** (2011) 374.

[15] M. Alexeev et al., *The quest for a third generation of gaseous photon detectors for Cherenkov imaging counters*, *Nucl. Instrum. Meth.* **A 610** (2009) 174; *THGEM based photon detector for Cherenkov imaging applications*, *Nucl. Instrum. Meth.* **A 617** (2010) 396; *Development of THGEM-based photon detectors for Cherenkov Imaging Counters*, 2010 *JINST* **5** P03009; *Progress towards a THGEM-based detector of single photons*, *Nucl. Instrum. Meth.* **A 639** (2011) 130; *Detection of single photons with THickGEM-based counters*, *Nucl. Instrum. Meth.* **A 695** (2012) 159; *Detection of single photons with ThickGEM-based counters*, 2012 *JINST* **7** C02014.

[16] A. Braem et al., *Results from the ageing studies of large CsI photocathodes exposed to ionizing radiation in a gaseous RICH detector*, *Nucl. Instrum. Meth.* **A 553** (2005) 187;
H. Hoedlmoser et al., *Long term performance and ageing of CsI photocathodes for the ALICE/HMPID detector*, *Nucl. Instrum. Meth.* **A 574** (2007) 28.

[17] E. Albrecht et al., *The radiator gas and the gas system of COMPASS RICH-1*, *Nucl. Instrum. Meth.* **A 502** (2003) 266.

[18] E. Albrecht et al., *The mirror system of COMPASS RICH-1*, *Nucl. Instrum. Meth.* **A 502** (2003) 236.

[19] P. Abbon et al., *Particle identification with COMPASS RICH-1*, *Nucl. Instrum. Meth.* **A 631** (2011) 26.

2014 JINST 9 P01006